The Journal of Chemical Physics

Electronic and vibrational relaxation dynamics of NH_3 Rydberg states probed by vacuum-ultraviolet time-resolved photoelectron imaging

Cite as: J. Chem. Phys. **151**, 104306 (2019); https://doi.org/10.1063/1.5116707
Submitted: 26 June 2019 . Accepted: 13 August 2019 . Published Online: 11 September 2019

Vít Svoboda, Chuncheng Wang, Max D. J. Waters, and Hans Jakob Wörner

The Journal of Chemical Physics ARTICLE scitation.org/journal/jcp

Electronic and vibrational relaxation dynamics of NH_3 Rydberg states probed by vacuum-ultraviolet time-resolved photoelectron imaging

Cite as: J. Chem. Phys. 151, 104306 (2019); doi: 10.1063/1.5116707
Submitted: 26 June 2019 • Accepted: 13 August 2019 •
Published Online: 11 September 2019

Vít Svoboda,[a] Chuncheng Wang,[a),b)] Max D. J. Waters,[a] and Hans Jakob Wörner[c]

AFFILIATIONS

Laboratory for Physical Chemistry, ETH Zürich, Vladimir-Prelog-Weg 2, 8093 Zürich, Switzerland

Note: This paper is part of the JCP Special Collection on Ultrafast Spectroscopy and Diffraction from XUV to X-ray.
[a]**Contributions:** V. Svoboda, C. Wang, and M. D. J. Waters contributed equally to this work.
[b]**Also at:** Institute of Atomic and Molecular Physics, Jilin University, Qianjin Street 2699, China.
[c]**Electronic mail:** hwoerner@ethz.ch. **URL:** www.atto.ethz.ch.

ABSTRACT

Time-resolved dynamics of high-lying Rydberg states of ammonia (NH_3) prepared by using a vacuum ultraviolet (VUV) pump (~9.3 eV) and an ultraviolet (UV) probe (~4.7 eV) pulse are reported using photoelectron imaging detection. After photoexcitation, two main features appear in the photoelectron spectrum with vertical binding energies of ~1.8 eV and ~3.2 eV and with distinctly different anisotropy parameters β of ~1.3 and ~0.7, respectively. This information allows the unambiguous assignment of the respective Rydberg states and disentangles the induced electronic and vibrational dynamics. The combination of velocity-map imaging with femtosecond VUV and UV pulses is shown to offer an attractive approach for studying the dynamics of high-lying Rydberg states of small molecules.

I. INTRODUCTION

Many spectroscopic and theoretical studies have been devoted to ammonia (NH_3).[1–5] Studies which have focused on electronically excited NH_3 have been mainly focused on the low-lying Rydberg states (~6 eV) investigating their complex photodissociation dynamics.[4,6,7] The few studies that have involved high-lying Rydberg states have been confined to static measurements[1,8,9] because of a lack of vacuum ultraviolet (VUV) femtosecond laser sources.

In many biologically relevant molecules, such as amino acids, the sp^3 hybridized nitrogen is the central functional unit in defining their photochemistry, e.g., through valence-Rydberg mixing that causes their surprising stability to UV light.[10,11] Further understanding of the mechanisms by which these nitrogen centers are able to efficiently redistribute absorbed UV light therefore has a natural imperative that invites further study. While there are certainly differences between the photoinduced molecular dynamics of C–N bonds and N–H bonds,[12] the study of small molecules can shed light on the fundamental dynamics of moieties that could be clouded by increased complexity, in addition to having the benefit of being accessible to state-of-the-art quantum-chemical calculations without facing extreme computational costs.

NH_3 makes an ideal candidate system as it is a small molecule with an sp^3 hybridized nitrogen center. Moreover, hydrogen substitution leads to the creation of nitrogen containing biomolecules, and its spectroscopy can be interpreted in terms of simple symmetry arguments. Due to this, many studies have been devoted to the spectroscopy of NH_3. The early works studying the photodissociation dynamics were pioneered by Ashfold and co-workers,[4,13–15] who paved the way for most of the subsequent interest in the $\tilde{A}$ state of NH_3. Since then, many research groups contributed to this effort.[15–19] However, these experiments were limited to static

studies, due to the lack of ultrashort pulses in the UV/VUV domain. Recently, table-top UV/VUV femtosecond sources emerged and have proven highly valuable for dynamical studies.[20–26] The natural evolution of this experimental effort in understanding the photophysics of NH_3 is then to use these femtosecond UV/VUV sources and investigate the time-resolved dynamics of the high-lying Rydberg states in NH_3.

In the present study, the dynamics of the high-lying Rydberg states of NH_3 are followed through time- and angle-resolved photoelectron spectroscopy. The states involved are fully characterized utilizing a time-resolved velocity-map-imaging (VMI) spectrometer with a VUV pump (133 nm) and a UV probe (266 nm). One of the strengths of VMI spectroscopy is that the technique allows one to capture the photoelectron spectrum while simultaneously obtaining the photoelectron angular distribution (PAD). This PAD is related to the orbital-angular-momentum character of the ejected photoelectron, which carries information about the corresponding character of the photoionized orbital. The time- and energy-dependencies of the PAD can assist the interpretation of the observed dynamics or even provide additional insights.

The presented study discusses the time-resolved Rydberg-state dynamics of NH_3 in the high-lying Rydberg states (~9.3 eV) and their ultrafast electronic and vibrational relaxation, probed via 266 nm pulses. This wavelength was chosen because it allows the relaxation dynamics to be followed over the set of intermediate states with higher vertical binding energies than the initially prepared states. The paper is organized as follows: Section II describes the experimental setup and summarizes the typical experimental conditions, followed by a brief description of the data analysis. Section III presents the results of time-resolved photoelectron spectra as well as the time- and angle-resolved photoelectron distributions. Section IV discusses the experimental results in terms of the assignment of individual Rydberg states and their anisotropy parameters β_2. The dynamics of these states are discussed in the framework of kinetic modeling providing the time constants for the involved processes. The conclusions are presented in Sec. V.

II. METHODS

A. Experimental

The experimental setup has been described in detail elsewhere.[23] The experiment is driven by 1.5 mJ 800 nm pulses from a Ti:Sa regenerative amplifier (Coherent Legend Elite Duo) with a pulse duration of 35 fs operating with a repetition rate of 1 kHz. The fundamental beam is passed through a 70:30 beam splitter to create two arms of the interferometer, with the transmitted component being used to generate the 266 nm probe through third-harmonic generation in nonlinear crystals and the reflected component used to generate the 133 nm pump, as follows. The 800 nm beam is frequency doubled using a 300 μm thick β-barium borate (BBO) crystal to generate a 400 nm beam. This beam is then spectrally filtered and focused on a semi-infinite gas cell for low-order harmonic generation. The third harmonic beam centered at 133 nm (~9.3 eV) is generated in xenon (~10 mbar). Afterward, the linearly (and parallel) polarized beams in both arms are spectrally filtered, time delayed with respect to each other using a motorized delay stage, and noncollinearly (crossing angle <1°) focused (f = 500 mm) onto the interaction region of a VMI spectrometer.

An Amsterdam pulsed valve (MassSpecpecD BV, 1 kHz repetition rate) using a piezocantilever opening mechanism[27–29] with 150 μm orifice and 40° degree conical nozzle shape for enhanced center-line intensity is used to generate the unseeded molecular beam of NH_3 (PanGas, purity 99.98%). The typical backing pressure is between 1 bar and 1.5 bar, and the pulse width of the valve is 40 μs. The molecular beam created by the nozzle is sent through a 1 mm skimmer and propagated 10 cm downstream to the interaction region where it is ionized by the combined action of the laser beams. The laser cross correlation (CC) was determined via (1 + 1′)-photon nonresonant ionization of xenon and is modeled as a Gaussian function with a full-width at half-maximum (FWHM) of 92(5) fs.

For each time step, four images are recorded: two images with only the pump or probe beam, one image with both beams, and one background image with no beam. Altogether, the whole time delay axis is measured 30 times with a single-image acquisition time of 20 s. The multiple images at each time step are background corrected and averaged. The pump-probe signal is obtained by subtracting single-color images from images recorded with both beams. The pump-probe images are then inverted using the MEVELER inversion method.[30]

III. RESULTS

Figure 1(a) shows the measured time-resolved photoelectron spectrum (TRPES) as a 2D map, i.e., as a function of the

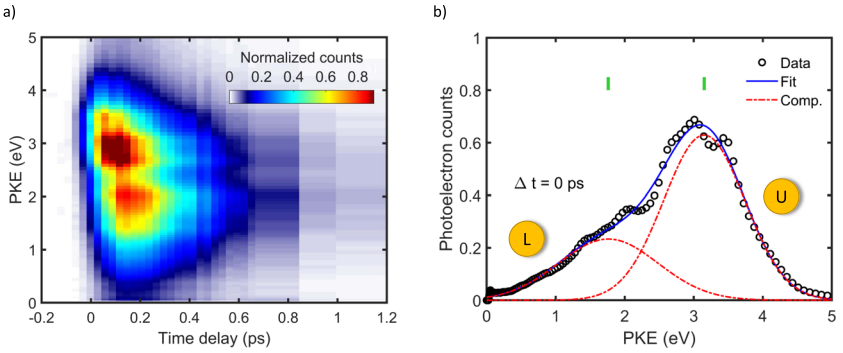

FIG. 1. Panel (a): Measured time-resolved photoelectron spectrum (TRPES) of NH_3. The spectrum has two main peaks on the positive-delay side. The normalized photoelectron counts are shown by the false-color map. Panel (b) is the slice of the TRPES at Δt = 0 ps. Black circles represent the measured data, and the blue solid line is the best fit with two Gaussian components shown by the red dashed-dotted lines. Green lines indicate the two center positions of the peaks.

photoelectron kinetic energy (PKE) and time delay (Δt) between the laser pulses. The positive time delay means that the pump pulse (133 nm) precedes the probe pulse (266 nm). The time-delay axis is scanned between −0.3 ps and 3.0 ps in nonequidistant steps, with a denser grid (step size = 30 fs) focusing around time zero. On the negative-delay side, there is no signal in the TRPES because NH_3 does not absorb around 266 nm.[31] All observed signals are due to the excitation by the pump pulse (~9.3 eV), resulting in two main features decaying within 600 fs after time zero. It is evident from the TRPES that the maxima of each of the two features are reached at different time delays and shifted with respect to time zero.

The TRPES clearly shows that the entire photoelectron signal is seen below 5 eV, which can be rationalized by considering that ultrafast photoelectron spectroscopy is measuring vertical transitions, and the first vertical ionization potential of NH_3 is 10.85 eV[32] (the adiabatic ionization potential is 10.19 eV),[33] and the total photon energy is ~14 eV which gives a maximum of PKE at ~3.15 eV; as no signals are observed above this PKE, multiphoton processes can be excluded. To obtain further insight into the observed TRPES, a time slice at time zero is taken and modeled by a sum of Gaussians [shown in Fig. 1(b)]. From the best fit (fitting parameters shown in Table I), two Gaussians centered at 1.76 eV and 3.15 eV are necessary to reproduce the spectrum. Additional Gaussians did not result in any improvement of the fit, confirming the two-feature interpretation of the TRPES. These two features are denoted with "U" and "L," corresponding to the features originating from the higher and lower PKE signals, respectively.

TABLE I. Fitting parameters from the best fit to the time-zero slice of the TRPES. For more details about the fit, see the main text.

Lower peak maximum	1.76 ± 0.15 eV
Lower peak FWHM	1.68 ± 0.12 eV
Upper peak maximum	3.15 ± 0.04 eV
Upper peak FWHM	1.38 ± 0.04 eV
R^2	0.9926
Root-mean-square error	0.0169

This is shown in Fig. 1(b) by the letters "U" and "L" in the yellow circles.

Figure 2(a) shows the result of the global fit of the measured TRPES. The fit relies on a time-slice analysis, where each time slice (representing static photoelectron spectra) is modeled by a sum of Gaussians. The advantage of this method is that no specific time dependence needs to be assumed. This differs from traditional approaches which model the time evolution as a sum of exponential decays convoluted with the instrument-response function. Moreover, the employed model allows for interpretation of a complex wavepacket evolution because the Gaussians at each time step can change both their positions as well as their widths. The relative difference between the measured TRPES and the fitted TRPES is always within a relative deviation of ±10%. The fit results in a separation of the measured signal into two components, which are shown in

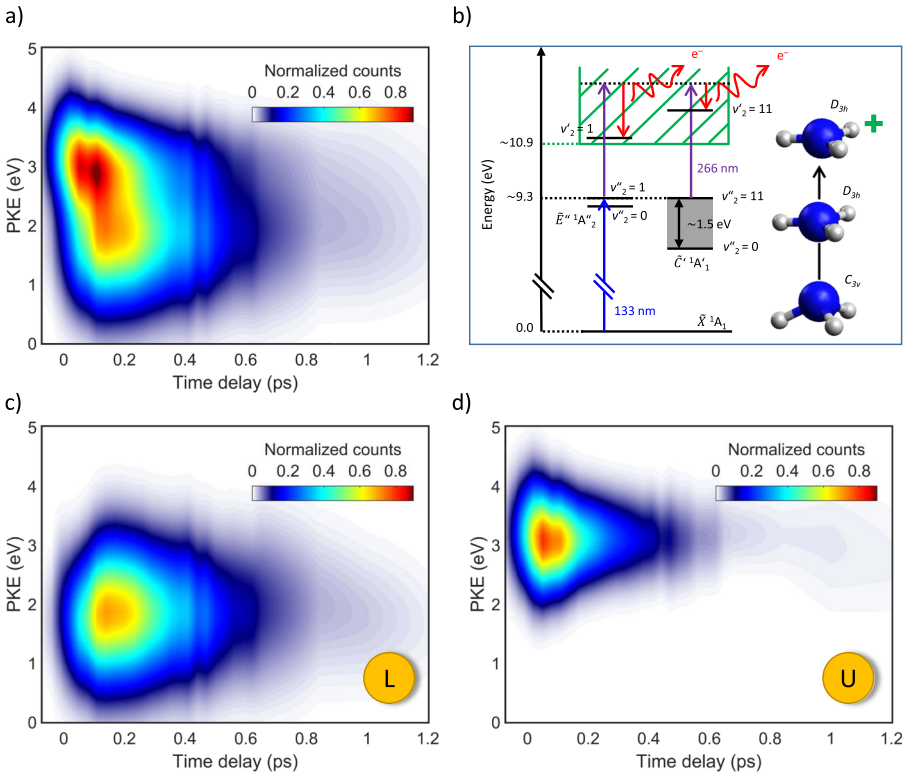

FIG. 2. Panel (a) shows a global fit of the measured TRPES created by analyzing each time slice with the two state model described in the text. Panels (c) and (d) show the two separated features corresponding to the lower and upper peaks from Fig. 1(b), respectively. Panel (b) shows the energy-level diagram of the involved states and the transitions between them, where the green hashed box is the photoelectron continuum associated with the electronic ground state of the cation, the solid black lines are the Rydberg states, the blue arrow is the photoexcitation with 133 nm light, the purple arrows represent photoionization induced by 266 nm, and the red arrows show the kinetic energy of ejected electrons. The equilibrium geometries of NH_3 in its ground state, Rydberg states, and the ground state of the ion are shown on the right-hand side of the energy level diagram.

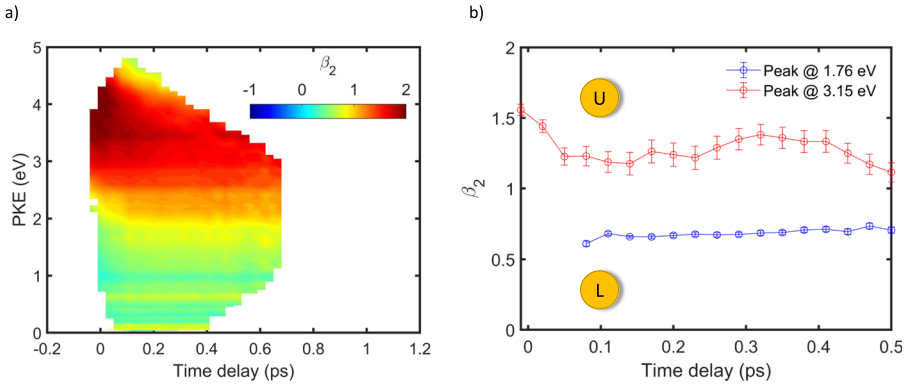

FIG. 3. Panel (a) shows the β_2 parameter map as a function of the time delay and PKE. The asymmetry parameter β_2 is shown in false-color representation. Panel (b) shows the peak-specific evolution of their respective $\beta_2^{(i)}(\Delta t)$ parameters.

Figs. 2(c) and 2(d) centered around PKE ~ 1.8 eV and PKE ~ 3.2 eV, respectively. Both components show no time-dependent change in the peak position, and the signal of both components decays to zero within less than 600 fs, albeit on two different timescales.

The time-dependent photoelectron angular distribution (PAD) is shown in Fig. 3(a) as a 2D map of the $\beta_2(\Delta t, \text{PKE})$ parameter in a false-color representation. In the white area, the photoelectron signal is too weak, ≲6% of its maximum, to get a reliable β_2 parameter; therefore, this area is excluded from further analysis. Looking at Fig. 3(a), two distinct regions of the β_2 parameter can be identified, one with a high anisotropy ($\beta_2 \to 2$) at PKE between 2 eV and 5 eV and a more isotropic ($\beta_2 \to 0$) region at PKE between 0 eV and 2 eV. The β_2 parameters are indicative of the angular momentum components of the ionized orbital.[34]

Figure 3(b) shows the time evolution of the $\beta_2^{(i)}(\Delta t)$ parameter for each component $i \in \{l, u\}$ from the TRPES, averaged over the peak width of the given component. For this, the energy-dependent distribution functions $Q_2(\text{PKE})$ for each time delay Δt, which are related to the Legendre polynomials $\mathscr{P}_2$ by

$$Q_2(\text{PKE}) \propto \int_0^{\pi} S(\text{PKE}, \theta) \cdot \mathscr{P}_2(\cos\theta) \cdot \sin\theta \mathrm{d}\theta, \qquad (1)$$

where $S(\text{PKE}, \theta)$ is the measured photoelectron image at a given time delay as a function of energy and angle, are calculated. As the photoelectron image is, in principle, a sum of the Q_2 functions due to different ionization channels, it is possible to separate the β_2 parameters of each channel by multiplying the β_2 map with the TRPES to obtain the distribution function Q_2. Then, the slice analysis is performed upon the Q_2 map to obtain the $Q_2^{(i)}$ functions. Dividing $Q_2^{(i)}$ by the component-specific TRPES, [see Figs. 2(c) and 2(d)], $\beta_2^{(i)}$ parameter maps for each component are obtained and hence, their time evolutions can be extracted.

Following Fig. 3(b), the $\beta_2^{(u)}$ parameter has an initial value of ~1.5 at time zero, indicating a strong anisotropy. The parameter then decays rapidly within the first 100 fs to a value of ~1.25. The $\beta_2^{(l)}$ parameter is impossible to evaluate before 100 fs, due to the photoelectron signal of this band being on the level of the noise. From this point onward, it is time-independent with a value of ~0.7.

IV. DISCUSSION

NH_3 in its electronic ground state is a pyramidal molecule with a low barrier along the umbrella-inversion mode resulting in a tunneling splitting of ~0.1 meV, which can be observed in high-energy-resolution experiments. If the tunneling splitting is resolved, the umbrella inversion is considered as "feasible" and the proper molecular-symmetry group in this case is D_{3h} (M).[35,36] In the present experiments, the energy resolution is not sufficient to resolve the tunneling splitting; hence, the ground state should be described in the C_{3v} group. However, the Rydberg states have a planar equilibrium geometry because they converge to the electronic ground state of NH_3^+ which is planar.[1] Therefore, the Rydberg states are described in the D_{3h} group, irrespective of the energy resolution.[1,37]

NH_3 is a small molecule with a central nitrogen atom in a "ligand-field" of three hydrogen atoms and is isoelectronic with Ne. Hence, it can be well described using the united-atom limit, allowing symmetry assignments of individual orbitals of NH_3 to be derived by a D_{3h} field splitting of the atomic orbitals of Ne (summarized in Table II). Consequently, s orbitals are of a_1' symmetry, p_z orbitals are of a_2'' symmetry (as they are antisymmetric with respect to the σ_h plane), and $p_{x,y}$ orbitals are e'. The d_{z^2} orbitals are totally symmetric; therefore, they have a_1' symmetry. $d_{xz,yz}$ orbitals are degenerate and antisymmetric with respect to the σ_h plane; therefore, they have e'' symmetry, and the d_{xy,x^2-y^2} orbitals are degenerate and have e' symmetry because they are symmetric with respect to the σ_h plane. The highest occupied molecular orbital of NH_3 is the nitrogen lone pair, having $2pa_2''$ symmetry. The dynamics presented here are those following single-photon excitation of one electron of the $2pa_2''$ orbital to a high-lying Rydberg state, converging to the cationic ground state, which is characterized by the ion core $(2pa_2'')^{-1}$.

TABLE II. Symmetry descent table from the spherical group R_3 to the point group D_{3h}.

R_3	D_{3h}
S	A_1'
P	$A_2'' + E'$
D	$A_1' + E' + E''$

Figure 1(b) shows two peaks centered at PKEs of 3.15 eV and 1.76 eV (see also Table I). In the energy range around ~9.3 eV, there are at least three Rydberg states $\tilde{E}''\,^1A_2''$, $\tilde{E}'''\,^1A_2''$, and $\tilde{F}^1E''$ which are accessible via one-photon excitation.[8,38] The former one is of s-character, whereas the remaining ones have d-character. Ionization of all three states would lead to a photoelectron with very similar PKE. The upper peak in the TRPES is assigned as the $\tilde{E}''$ state based on its PKE and its PAD [Fig. 3(a)], which is consistent with a Rydberg state of *s* character, making contributions from other states very unlikely, because they would result in a more isotropic PAD.

Previous work by Langford *et al.*[1] observed four Rydberg states in the vicinity of 9.3 eV: $\tilde{B}\,^1E''$, $\tilde{C}'\,^1A_1'$, $\tilde{E}'^1A_1'$, and $\tilde{E}''\,^1A_2''$, using two-photon excitation. In contrast to single-photon excitation under which the first three states are dipole forbidden (in the atomic limit) because they are of *p* character, in two-photon excitation, the dipole selection rules are less restrictive and hence these states are observed. Since the $\tilde{E}''$ state is dipole forbidden in two-photon excitation, it appears as a very weak transition in the work by Langford *et al.*[1]

The assignment of the lower band in TRPES is slightly more involved. The band is centered at 1.76 eV, which is consistent with ionization of the $\tilde{C}'$ state.[8,38] This assignment is additionally supported by the observed PADs, which display an anisotropy consistent with a *p*-type Rydberg state. However, single-photon excitation of a *p* state is dipole forbidden in the atomic limit. This suggests that the $\tilde{C}'$ state is populated through internal conversion, mediated by strong vibronic coupling between the $\tilde{E}''$ state and the $\tilde{C}'$ state. This interpretation is supported by the delayed rise of the signal of the $\tilde{C}'$ state with respect to the $\tilde{E}''$ state and also by the time-dependent change in the asymmetry parameters of the two states.

As is visible in Fig. 2, the photoelectron signals corresponding to the $\tilde{E}''$ and $\tilde{C}'$ states evolve differently in time. This is even better visible in Fig. 4, which shows the energy-integrated signal of each peak, as obtained from the fitting procedure discussed above [see Figs. 2(c) and 2(d)]. It is clear from Fig. 4 that the signal maximum of each state is offset from time zero, located at the maximum of the cross correlation curve. A reasonable fit of the $\tilde{E}''$ state is obtained by assuming a mono-exponential decay of the population,

$$f(t) = A \cdot e^{-\frac{t}{\tau_1}} \otimes g(t), \tag{2}$$

where $g(t)$ is the measured cross correlation function (shown in each panel of Fig. 4 as the red dotted-dashed line) and τ_1 is the decay time of the state. However, this does not provide a good fit of the $\tilde{C}'$-state signal. Therefore, a first-order sequential kinetic model is assumed,

$$f(t) = \left\{ \left[\frac{\left(\frac{P}{\tau_R}\right)}{\frac{1}{\tau_R} - \frac{1}{\tau_D}} \right] \cdot \left(e^{-\left(\frac{t}{\tau_D}\right)} - e^{-\left(\frac{t}{\tau_R}\right)} \right) \right\} \otimes g(t), \tag{3}$$

where τ_R gives the rise time of the state population and τ_D is its decay. Figure 2(b) shows a schematic energy level diagram illustrating the proposed dynamics. Excitation of the ground state by 133 nm light prepares the $\tilde{E}''$ state, which then decays to the $\tilde{C}'$ state due to strong vibronic coupling that is likely mediated via the umbrella mode.

The time constants obtained from the fits are shown in Fig. 4 and summarized in Table III. The $\tilde{E}''$ signal reaches its maximum within the cross correlation time, meaning that the state is directly excited by the pump pulse. This state then decays on an ultrafast time scale with τ_1 of ~150 fs. This time constant is shorter than the expected lifetime based on the linewidths from the high-resolution spectra.[1] The time constant must therefore represent the evolution of the photoexcited wavepacket from the initial Franck-Condon region to a configuration space where either the wavepacket cannot be energetically ionized by one photon of 266 nm or the ionization probability drops to zero for other reasons.

Contrary to the $\tilde{E}''$ state, the photoelectron signal of the $\tilde{C}'$ state has a rise time of ~86 fs. This observed rise is likely a consequence of ultrafast population transfer from a higher state, meaning that the initially prepared wavepacket on the $\tilde{E}''$ state populates the $\tilde{C}'$ state via internal conversion, most likely mediated by a conical intersection. After this, the photoelectron signal decays on an ultrafast time scale of 200 fs, for similar reasons as previously discussed.

The population transfer via internal conversion is supported by the time dependence of the anisotropy parameters, as is shown in Fig. 3(b). This change is indicative of strong vibronic coupling between these two states, which can be rationalized with symmetry arguments by considering the D_{3h} point group. The upper state ($\tilde{E}''$) is an *s*-type Rydberg state, so the ejected photoelectron would be expected to display a strong anisotropy, which is seen at time zero. This anisotropy becomes weaker in the first 100 fs, before remaining

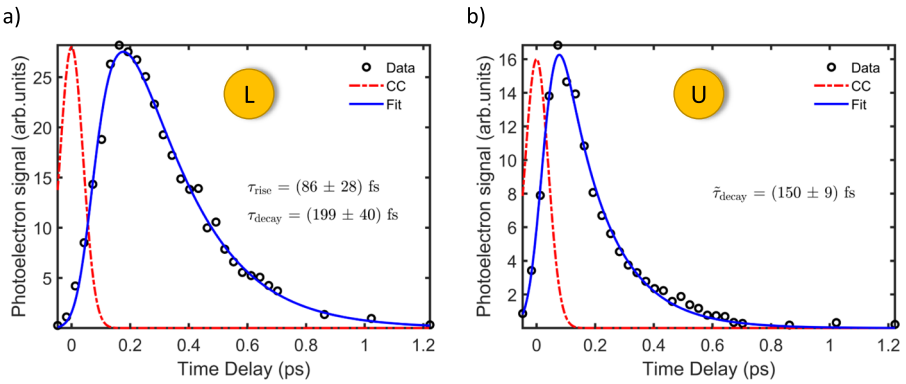

FIG. 4. Plots showing the 1D decay of each peak from Fig. 2, and the different kinetic models used to fit them (blue line). A first-order sequential model is assumed to fit the lower peak as shown in panel (a). Panel (b) shows a mono-exponential fit of the upper peak. The experimental cross correlation (CC) is shown with the red dotted-dashed line.

TABLE III. Fitted rise and decay times for the upper and the lower peaks.

Peak	State	τ_R (fs)	τ_D (fs)	Model
Upper	$\tilde{E}''\,^1A_2''$	...	150 ± 9	Monoexponential fit
Lower	$\tilde{C}'\,^1A_1'$	86 ± 28	199 ± 40	Sequential kinetic model

more or less stable at ~1.2. The lower state ($\tilde{C}'$) is a *p*-type Rydberg state, which would lead to *s* and *d* partial waves upon photoionization. Depending on the mixing of the two, the PAD could be expected to be nearly isotropic. The observed PAD is not isotropic and has a time-independent value of ~0.7. This suggests that the ($\tilde{C}'$) state is mixed with the $\tilde{E}''$ state, due to the population transfer. This behavior is consistent with previous observations of ultrafast internal conversion, mediated by a conical intersection.[39]

The observed coupling between the $\tilde{E}''$ and $\tilde{C}'$ states is likely due to the umbrella mode. The NH_3 umbrella mode has A_2'' symmetry, meaning that this motion is allowed to mediate the relaxation process $\tilde{E}'' \rightarrow \tilde{C}'$.[40] The observed change in the PAD for the ($\tilde{E}''$) state is due to this vibronic coupling between the two states, resulting in neither state being purely of *s* or *p* character, but instead having a mixed *s*/*p* character.[39,41] The assumption that the umbrella mode would be the coordinate of interest is justified by the equilibrium geometries of the ground state and Rydberg states of NH_3, meaning that it is the umbrella mode that takes the system out of the Franck-Condon region, which would also explain the ultrafast population transfer to the $\tilde{C}'$ state.

V. CONCLUSIONS

Our time-resolved photoelectron imaging experiment of the high-lying Rydberg states of NH_3, accessed by a table-top VUV light source, shows an ultrafast population transfer from the $\tilde{E}''$ state to the $\tilde{C}'$ state due to internal conversion mediated by the umbrella motion. The $\tilde{E}''$ state is directly populated with the pump pulse and decays on the order of ~150 fs. Afterward, the ultrafast population transfer to the $\tilde{C}'$ state occurs within <100 fs, and the state as a whole is shown to undergo ultrafast decay within ~200 fs. The angular information obtained by using VMI allows these states to be unambiguously assigned on the basis of the anisotropy parameters and the kinetic energy of the ejected photoelectrons, allowing one to track the evolution of the prepared wavepacket. The interpretation presented is only made possible by knowing the time evolution of the PAD as the key information is the mixed character of each state evident from the time-dependent anisotropy of the ejected photoelectrons. This demonstrates the strength of VMI in time-resolved studies, especially in cases where the complex dynamics are presented and both energy- and angular-distributions are needed for unambiguous assignments.

ACKNOWLEDGMENTS

We acknowledge financial support from ETH Zürich and the Swiss National Science Foundation through Grant No. 200021_172946. C.W. additionally acknowledges support from the National Natural Science Foundation of China (Grant Nos. 11534004, 11627807, and 11774130).

REFERENCES

[1] S. R. Langford, A. J. Orr-Ewing, R. A. Morgan, C. M. Western, M. N. R. Ashfold, A. Rijkenberg, C. R. Scheper, W. J. Buma, and C. A. de Lange, "The spectroscopy of high Rydberg states of ammonia," J. Chem. Phys. **108**, 6667–6680 (1998).
[2] V. Svoboda, J. Rakovský, and O. Votava, "New insight on ammonia 1.5 μm overtone spectra from two-temperature analysis in supersonic jet," J. Quant. Spectrosc. Radiat. Transfer **227**, 201–210 (2019).
[3] G. C. Nieman and S. D. Colson, "A new electronic state of ammonia observed by multiphoton ionization," J. Chem. Phys. **68**, 5656–5657 (1978).
[4] D. H. Mordaunt, M. N. R. Ashfold, and R. N. Dixon, "Photodissociation dynamics of a state ammonia molecules. I. State dependent μ-ν correlations in the $NH_2(ND_2)$ products," J. Chem. Phys. **104**, 6460–6471 (1996).
[5] C. Xie, J. Ma, X. Zhu, D. H. Zhang, D. R. Yarkony, D. Xie, and H. Guo, "Full-dimensional quantum state-to-state nonadiabatic dynamics for photodissociation of ammonia in its A-band," J. Phys. Chem. Lett. **5**, 1055–1060 (2014).
[6] H. Yu, N. L. Evans, A. S. Chatterley, G. M. Roberts, V. G. Stavros, and S. Ullrich, "Tunneling dynamics of the NH_3 ($\tilde{A}$) state observed by time-resolved photoelectron and H atom kinetic energy spectroscopies," J. Phys. Chem. A **118**, 9438–9444 (2014).
[7] M. Ashfold, C. Bennett, and R. Dixon, "Predissociation dynamics of $\tilde{A}$-state ammonia probed by two-photon excitation spectroscopy," Chem. Phys. **93**, 293–306 (1985).
[8] D. T. Cramb and S. C. Wallace, "Rydberg states near the ionization continuum: Autoionization in ammonia," J. Chem. Phys. **101**, 6523–6528 (1994).
[9] X. Li and C. R. Vidal, "Predissociation supported high-resolution vacuum ultraviolet absorption spectroscopy of excited electronic states of NH_3," J. Chem. Phys. **101**, 5523–5528 (1994).
[10] M. N. R. Ashfold, G. A. King, D. Murdock, M. G. D. Nix, T. A. A. Oliver, and A. G. Sage, "$\pi\sigma^*$ excited states in molecular photochemistry," Phys. Chem. Chem. Phys. **12**, 1218–1238 (2010).
[11] G. M. Roberts and V. G. Stavros, "The role of $\pi\sigma^*$ states in the photochemistry of heteroaromatic biomolecules and their subunits: Insights from gas-phase femtosecond spectroscopy," Chem. Sci. **5**, 1698–1722 (2014).
[12] L. B. Klein, J. O. F. Thompson, S. W. Crane, L. Saalbach, T. I. Sølling, M. J. Paterson, and D. Townsend, "Ultrafast relaxation dynamics of electronically excited piperidine: Ionization signatures of Rydberg/valence evolution," Phys. Chem. Chem. Phys. **18**, 25070–25079 (2016).
[13] J. Biesner, L. Schnieder, J. Schmeer, G. Ahlers, X. Xie, K. H. Welge, M. N. R. Ashfold, and R. N. Dixon, "State selective photodissociation dynamics of A state ammonia. I," J. Chem. Phys. **88**, 3607–3616 (1988).
[14] J. Biesner, L. Schnieder, G. Ahlers, X. Xie, K. H. Welge, M. N. R. Ashfold, and R. N. Dixon, "State selective photodissociation dynamics of A state ammonia. II," J. Chem. Phys. **91**, 2901–2911 (1989).
[15] D. H. Mordaunt, M. N. R. Ashfold, and R. N. Dixon, "State to state recoil anisotropies in the photodissociation of deuterated ammonia," J. Chem. Phys. **109**, 7659–7662 (1998).
[16] K. L. Wells, G. Perriam, and V. G. Stavros, "Time-resolved velocity map ion imaging study of NH_3 photodissociation," J. Chem. Phys. **130**, 074308 (2009).
[17] N. L. Evans, H. Yu, G. M. Roberts, V. G. Stavros, and S. Ullrich, "Observation of ultrafast NH_3 ($\tilde{A}$) state relaxation dynamics using a combination of time-resolved photoelectron spectroscopy and photoproduct detection," Phys. Chem. Chem. Phys. **14**, 10401–10409 (2012).
[18] A. S. Chatterley, G. M. Roberts, and V. G. Stavros, "Timescales for adiabatic photodissociation dynamics from the A state of ammonia," J. Chem. Phys. **139**, 034318 (2013).
[19] J. D. Rodríguez, M. G. González, L. Rubio-Lago, and L. Bañares, "A velocity map imaging study of the photodissociation of the A state of ammonia," Phys. Chem. Chem. Phys. **16**, 406–413 (2014).
[20] M. Beutler, M. Ghotbi, F. Noack, and I. V. Hertel, "Generation of sub-50-fs vacuum ultraviolet pulses by four-wave mixing in argon," Opt. Lett. **35**, 1491–1493 (2010).

[21] T. Horio, R. Spesyvtsev, and T. Suzuki, "Simultaneous generation of sub-20 fs deep and vacuum ultraviolet pulses in a single filamentation cell and application to time-resolved photoelectron imaging," Opt. Express **21**, 22423–22428 (2013).
[22] A. von Conta, M. Huppert, and H. J. Wörner, Rev. Sci. Instrum. **87**, 073102 (2016).
[23] V. Svoboda, N. B. Ram, R. Rajeev, and H. J. Wörner, "Time-resolved photoelectron imaging with a femtosecond vacuum-ultraviolet light source: Dynamics in the $\tilde{A}/\tilde{B}$- and $\tilde{F}$-bands of SO_2," J. Chem. Phys. **146**, 084301 (2017).
[24] A. von Conta, A. Tehlar, A. Schletter, Y. Arasaki, K. Takatsuka, and H. J. Wörner, Nature Commun. **9**, 3162 (2018).
[25] S. Adachi, M. Sato, T. Suzuki, and S. Y. Grebenshchikov, "Unexpectedly broad photoelectron spectrum as a signature of ultrafast electronic relaxation of Rydberg states of carbon dioxide," Phys. Rev. A **95**, 033422 (2017).
[26] T. Suzuki, "Femtosecond time-resolved photoelectron imaging," Annu. Rev. Phys. Chem. **57**, 555–592 (2006).
[27] D. Irimia, R. Kortekaas, and M. H. M. Janssen, "*In situ* characterization of a cold and short pulsed molecular beam by femtosecond ion imaging," Phys. Chem. Chem. Phys. **11**, 3958–3966 (2009).
[28] D. Irimia, D. Dobrikov, R. Kortekaas, H. Voet, D. A. van den Ende, W. A. Groen, and M. H. M. Janssen, "A short pulse (7 μs FWHM) and high repetition rate (DC-5KHz) cantilever piezovalve for pulsed atomic and molecular beams," Rev. Sci. Instrum. **80**, 113303 (2009).
[29] C. Meng and M. H. M. Janssen, "Measurement of the density profile of pure and seeded molecular beams by femtosecond ion imaging," Rev. Sci. Instrum. **86**, 023110 (2015).
[30] B. Dick, "Inverting ion images without Abel inversion: Maximum entropy reconstruction of velocity maps," Phys. Chem. Chem. Phys. **16**, 570–580 (2014).
[31] J. A. Syage, R. B. Cohen, and J. Steadman, "Spectroscopy and dynamics of jet-cooled hydrazines and ammonia. I. Single-photon absorption and ionization spectra," J. Chem. Phys. **97**, 6072–6084 (1992).
[32] K. Kimura, *Handbook of HeI Photoelectron Spectra of Fundamental Organic Molecules: Ionization Energies, Ab Initio Assignments, and Valence Electronic Structure for 200 Molecules* (Halsted Press, 1981).
[33] W. Habenicht, G. Reiser, and K. Müller-Dethlefs, "High-resolution zero kinetic energy electron spectroscopy of ammonia," J. Chem. Phys. **95**, 4809–4820 (1991).
[34] K. L. Reid, "Photoelectron angular distributions," Annu. Rev. Phys. Chem. **54**, 397–424 (2003).
[35] P. R. Bunker and P. Jensen, *Molecular Symmetry and Spectroscopy*, 2nd ed. (NRC Press, Ottawa, Canada, 1998), ISBN: 0-660-17519-3.
[36] S. Urban, "High-resolution infrared spectroscopy of ammonia: A survey of theory and analyses of spectra," J. Quant. Spectrosc. Radiat. Transfer **48**, 675–684 (1992).
[37] M. Ashfold, S. Langford, R. Morgan, A. Orr-Ewing, C. Western, C. Scheper, and C. de Lange, "Resonance enhanced multiphoton ionization (REMPI) and REMPI-photoelectron spectroscopy of ammonia," Eur. Phys. J. D **4**, 189–197 (1998).
[38] J. H. Glownia, S. J. Riley, S. D. Colson, and G. C. Nieman, "The MPI spectrum of expansion-cooled ammonia: Photophysics and new assignments of electronic excited states," J. Chem. Phys. **73**, 4296–4309 (1980).
[39] R. A. Livingstone, J. O. F. Thompson, M. Iljina, R. J. Donaldson, B. J. Sussman, M. J. Paterson, and D. Townsend, "Time-resolved photoelectron imaging of excited state relaxation dynamics in phenol, catechol, resorcinol, and hydroquinone," J. Chem. Phys. **137**, 184304 (2012).
[40] H. Köppel, W. Domcke, and L. S. Cederbaum, *Advances in Chemical Physics* (John Wiley & Sons, 2007), pp. 59–246, https://onlinelibrary.wiley.com/doi/pdf/10.1002/9780470142813.ch2.
[41] T. Horio, T. Fuji, Y.-I. Suzuki, and T. Suzuki, "Probing ultrafast internal conversion through conical intersection via time-energy map of photoelectron angular anisotropy," J. Am. Chem. Soc. **131**, 10392–10393 (2009).